HHS Public Access

Author manuscript

*Nanomedicine*. Author manuscript; available in PMC 2025 May 20.

Published in final edited form as:

*Nanomedicine*. 2025 April ; 65: 102812. doi:10.1016/j.nano.2025.102812.

# Nanogels conjugated with cell-penetrating peptide as drug delivery vehicle for treating urinary tract infections

**Humberto D. Escobedo, Ph.D**[a], **Nicholas Zawadzki, BS**[b], **James K.A. Till, Ph.D**[c], **Andres Vazquez-Torres, D.V.M., Ph.D**[c,d], **Guankui Wang, Ph.D**[a], **Dmitri Simberg, Ph.D**[a], **David J. Orlicky, Ph.D**[e], **Joshua Johnson, Ph.D**[b], **Marsha K. Guess, MD, MS**[b], **Devatha P. Nair, Ph.D**[f], **Michael J. Schurr, Ph.D**[c,*]

[a]Department of Pharmaceutical Science, Skaggs School of Pharmacy and Pharmaceutical Sciences, University of Colorado Anschutz Medical Campus, Aurora, CO 80045, USA

[b]Department of Obstetrics and Gynecology, School of Medicine, University of Colorado Anschutz Medical Campus, Aurora, CO 80045, USA

[c]Department of Immunology and Microbiology, School of Medicine, University of Colorado Anschutz Campus, Aurora, CO 80045, USA

[d]Veterans Affairs Eastern Colorado Health Care System, Denver, CO, USA

[e]Department of Pathology, School of Medicine, University of Colorado Anschutz Campus, Aurora, CO 80045, USA

[f]Department of Craniofacial Biology, School of Dental Medicine, University of Colorado Anschutz Medical Campus, Aurora, CO 80045, USA

## Abstract

Among hospital–acquired infections, *Pseudomonas aeruginosa*-associated urinary tract infections (UTIs) are mainly caused by indwelling urethral catheters (catheter-associated UTIs or CAUTIs) and are difficult to treat, resulting in high rates of morbidity among hospitalized patients. While antibiotics can successfully treat bacteria in the bladder lumen, they are inefficient at crossing stratified urothelium plasma membranes to kill persistent intracellular bacterial communities



*Corresponding author at: 12800 E. 19th Avenue, Research I North, Mail Stop 8333, Aurora, CO 80045, USA. MICHAEL.SCHURR@CUANSCHUTZ.EDU (M.J. Schurr).

CRediT authorship contribution statement

**Humberto D. Escobedo:** Writing – review & editing, Writing – original draft, Visualization, Validation, Supervision, Project administration, Methodology, Investigation, Formal analysis. **Nicholas Zawadzki:** Writing – original draft, Validation, Investigation, Formal analysis. **James K.A. Till:** Writing – original draft, Methodology, Investigation, Formal analysis. **Andres Vazquez-Torres:** Writing – review & editing, Resources, Funding acquisition. **Guankui Wang:** Resources. **Dmitri Simberg:** Writing – review & editing, Resources, Funding acquisition, Conceptualization. **David J. Orlicky:** Writing – review & editing, Resources, Methodology. **Joshua Johnson:** Writing – review & editing, Methodology. **Marsha K. Guess:** Writing – review & editing, Resources, Methodology, Funding acquisition, Conceptualization. **Devatha P. Nair:** Writing – review & editing, Supervision, Resources, Funding acquisition, Conceptualization. **Michael J. Schurr:** Writing – review & editing, Supervision, Resources, Methodology, Funding acquisition, Conceptualization.

Declaration of competing interest

No conflict of interest was reported by the authors of this paper.

Appendix A. Supplementary data

Supplementary data to this article can be found online at https://doi.org/10.1016/j.nano.2025.102812.

(IBCs). Herein, we introduce an approach to target UTI IBCs by locally delivering the antibiotic gentamicin via polymeric nanogels conjugated with a cell-penetrating peptide Cys-Gly-Lys-Arg-Lys. This novel approach delivered ~36 % more intracellular gentamicin compared to drug delivered in solution in vitro. In an acute UTI murine model, the nanogel cell-penetrating peptide drug delivery system facilitated the transport of gentamicin into the urothelium and resulted in >90 % clearance of a uropathogenic *P. aeruginosa* clinical strain in vivo.

### Keywords

Nanogel; Drug delivery; Urinary tract infection; Cell penetrating peptide

## Introduction

Urinary tract infections (UTIs) are some of the most common and impactful infections seen in both inpatient and outpatient settings. UTIs disproportionally affect children, women, and the elderly and are responsible for a significant worldwide economic burden.[1,2] In addition to medical costs, patients who suffer from UTIs typically experience a compromised quality of life.[3] Left untreated, UTIs can cause kidney damage, sepsis, and even death.[4]

Uncomplicated UTIs are commonly caused by uropathogenic *Escherichia coli*. However, rising rates of *Pseudomonas aeruginosa* (*P. aeruginosa*) infections have been reported in recurrent UTIs (rUTIs), hospital-acquired UTIs, and catheter-associated UTIs (CAUTIs).[5,6] *P. aeruginosa* can invade the urothelium and survive intracellularly via the formation of persistent intracellular bacterial communities (IBCs).[7,8] While antibiotic regimens can successfully treat bacteria in the bladder lumen, they are typically inefficient in crossing the stratified urothelium plasma membranes, making *P. aeruginosa* IBCs difficult to treat. Repeated use of antibiotic therapies has also contributed to the growing bacterial resistance, resulting in higher morbidities.[4,8] There is an urgent need to develop alternative treatment strategies to treat and combat UTIs and rUTIs. Drug delivery modalities that can effectively deliver therapeutics by crossing urothelial plasma membranes to access IBCs may provide an effective mechanism of eliminating UTIs while curbing the excessive use of antibiotics to fight infections.

Previous studies have assessed the efficacy of nanoparticles (e.g., carbon-, metallic-, and lipid-based materials) for drug delivery for UTI treatment.[9–11] Although they have reduced bacterial infection, the relatively large size (100 nm – 500 nm), morphology, and rigidity of these particles prevents them from crossing membranes and stratified cell layers. In contrast, polymeric nanogels can be synthesized as soft, spherical, crosslinked networks that can reversibly swell and collapse.[12–14] Furthermore, nanogels are more biocompatible than nanoparticles, have a flexible size under 100 nm, and are able to encapsulate, stabilize, and deliver a wide range of therapeutics in a targeted manner.[12] Our group has extensively studied the parameters that control the size, morphology, and surface properties by monomer selection and choice of solvent/solvent volume that can facilitate small-molecule delivery in highly tailored, biocompatible nanogels.[15] Additionally, our previous work has shown that intravesically (I-VESIC)-delivered nanogels conjugated with the cell-penetrating peptide

(CPP), Cys-Gly-Lys-Arg-Lys (CGKRK), successfully penetrate the urothelial cells at multiple levels and deliver encapsulated contents in a healthy murine model.[16] Yet, to our knowledge, no extensive work has reported the use of targeted nanogels with a CPP for antibiotic delivery in a UTI treatment model.

Hence, we created a biocompatible nanogel conjugated with CPP that could be used as I-VESIC drug delivery vehicles to meet the challenge of delivering an antibiotic directly into urothelial cells in order to target IBCs in a UTI murine model. In this study, we selected the hydrophilic antibiotic gentamicin (GEN), owing to its long-considered impermeability to urothelial cell membranes.[17] This study aimed to determine the efficacy and feasibility of specially designed nanogels conjugated with CPP to encapsulate GEN, cross the urothelial cell plasma membranes, and deliver therapeutic doses to eradicate *P. aeruginosa* IBCs in vitro and in an acute UTI murine model.

## Materials and methods

### Nanogel synthesis and CPP conjugation

Following the protocol from a previously studied nanogel, 2-**h**ydroxyethyl acrylate, **t**etraethyl dimethacrylate, and **a**crylic acid monomers in 4× solvent ratio at ~70 % double-bond conversion (HTA) was synthesized for this study via a one-pot, solution-based, free-radical polymerization with a thermal initiator.[15] A detailed description is found in the Supplemental Information. HTA and CPP (synthesized by GenScript, Piscataway, NJ, USA) ($3.8 \times 10^{-3}$ wt%) were covalently linked with the residual acrylates on the HTA ($1.3 \times 10^{-3}$ CPP unit per HTA) via thiol-acrylate Michael addition reaction as previously done by using 100 μL of trimethylamine as the catalyst in phosphate-buffered saline at pH ~7 (PBS) for 16 h while stirring.[16] Afterward, any residual acrylate functionality present was reacted with 2-mercaptoethanol in excess, then dialyzed (MWCO 10 kDa, cellulose membrane) against deionized water and lyophilized.

### HTA-CPP nanogel characterization

The HTA molecular weight was determined by gel permeation chromatography (Viscoteck-270) with tetrahydrofuran (0.35 μL/min) as the mobile phase.[15] Additionally, the HTA-CPP size and zeta potential of HTA and HTA-CPP (0.5 mg/mL in PBS) were determined by dynamic light scattering using Zetasizer NanoZS (ZEN 3600, Malvern, Germany).

### GEN loading into HTA and HTA-CPP nanogels

To load GEN (Chem-Impex International; Wood Dale, IL) into HTA and HTA-CPP, a 20 % (w/v) of each at 40 mg/mL GEN solution dispersed in PBS was mixed overnight. For loading HTA-CPP with tritiated GEN (GEN*), a 20 % (w/v) of HTA-CPP was incubated in 100 μCi/mL of GEN* instead. The GEN-loaded HTA-CPP and HTA nanogels (HTA-CPP + GEN, HTA + GEN, and HTA-CPP + GEN* respectively) were isolated and dried from the free antibiotic after two 1 mL Milli-Q washes within a centrifugal filter (MWCO 10 kDa, polyether sulfone membrane). The filtrate in the collection tube was kept.

## Loading capacity and encapsulation efficiency

Following a published protocol, the GEN was collected as the filtrate was fluorescently derivatized with *o*-phthalaldehyde and quantified against a standard curve.[18] Fluorescence measurements (excitation ($\lambda_{ex}$) = 340 nm; emission ($\lambda_{em}$) = 455 nm) were done on the Synergy™ 4 multi-mode microplate reader. The drug loading capacity and encapsulation efficiency of GEN in HTA-CPP + GEN and HTA + GEN were calculated with two equations where α is the total mass of GEN introduced to the nanogel for loading, β is the quantified mass of GEN that remained unloaded, and is the total mass of nanogel used for drug loading[19]:

$$Loading\ \ Capacity(\%) = \frac{\alpha - \beta}{\sigma} \times 100 \quad (1)$$

$$Encapsulation\ \ Efficiency(\%) = \frac{\alpha - \beta}{\alpha} \times 100 \quad (2)$$

## GEN release kinetics

GEN release from the HTA-CPP + GEN and HTA + GEN was monitored via dialysis.[20] Briefly, GEN release was monitored from a dialysis tube (MWCO 10 kDa, cellulose membrane) at a volume of 400 μL with a concentration of 1 mg/mL of the total weight of the HTA-CPP + GEN and HTA + GEN within a 40 mL PBS reservoir at 37 °C with stirring. At 4-, 6-, 8-, 12-, 24-, and 96-h, samples from the reservoir were collected. The total sample volume removed by the four-hour timepoint was replaced with new PBS. GEN was quantified using the *o*-phthalaldehyde derivatization method described previously.[18]

## Cell viability by MTT assay

A human carcinoma urothelial cell line was used in this study (ATCC® HTB-9). The HTB-9 cells were grown with Roswell Park Memorial Institute (RPMI) 1640 medium supplemented with 10 % (v/v) fetal bovine serum. Cells were maintained at 37 °C with 5 % $CO_2$ until they reached ~70 % confluency and were trypsinized (0.25 % v/v trypsin) and sub-cultured.

The HTB-9 cells were seeded ~$1 \times 10^4$ cells per well and grown to confluency (> 90 %) in a 96-well plate with complete RPMI medium. The filter-sterilized (0.22 μm) HTA-CPP were introduced to the cells in complete RPMI medium at increasing concentrations (0 μg – 10,000 μg) and incubated at 37 °C with 5 % $CO_2$ for 24 h. The introduction of 1 % (v/v) Triton X-100 was used as a positive control. The negative control was cells without the presence of HTA-CPP (0 μg). Cell viability was determined by 3-[4,5-dimethylthiazole-2-yl]-2,5-diphenyltetrazolium bromide (MTT) assay.[21] Briefly, the cells were washed three times with Dulbecco's PBS, supplemented with calcium and magnesium, followed by adding 0.5 mg/mL of the tetrazolium dye in RMPI medium and incubating for 1 h at 37 °C with 5 % $CO_2$. An equal volume of RMPI medium was added with acidified isopropanol

(4 mM HCl, 1 % (v/v) Triton X-100) and incubated for 15 min on the orbital shaker. The absorbance was measured at 570 nm.

### GEN* uptake in human urothelial cells

The HTA-CPP + GEN* was resolubilized in 50 % (v/v) dimethyl sulfoxide in Dulbecco's Modified Eagle Medium to a final volume of 300 μL. Radioactivity of GEN* was measured in counts-per-minute using a scintillation counter. HTA-CPP + GEN* was added to HTB-9 cells to an approximate concentration of at least 1 μCi/mL for a total of 0.3 μCi per well. Concurrently, free GEN* was added to cells at a concentration normalized to counts-per-minutes of the HTA-CPP + GEN* to a concentration of approximately 0.7 μCi/mL. At 4 h, media from two samples was collected and placed into 5 mL of scintillation fluid to confirm equal treatment levels in terms of total radioactivity. Cells were washed one time with 1 mL of PBS with 12.5 μg/mL cold GEN. The cells were trypsinized (0.25 % v/v trypsin) at 37 °C for 5 min. Trypsinized cells were collected by centrifugation at 4,000 RPM for 5 min. The cell pellet was resuspended in 300 μL PBS and then added to 5 mL of scintillation fluid. Tritium counts were averaged over one minute for each sample. Counts were corrected for background.

### Bacterial strain, plasmids, media, and culture conditions

The uropathogenic *P. aeruginosa* clinical strain, UR34, was obtained from Dr. Alan Hauser at Feinberg School of Medicine in Northwestern University. The plasmid pMRP-1 was introduced into UR34 by electroporation to create UR34-GFP.[22] UR34-GFP growth medium was Lysogeny Broth (LB; 10 g/L casein peptone, 5 g/L yeast extract, and 5 g/L sodium chloride).

For the acute UTI model, UR34-GFP were grown statically in 2 mL of LB for 10 h at 37 °C. The bacteria were collected by centrifugation from the broth and resuspended in PBS to ~1 × $10^9$ colony-forming-unit (CFU) per milliliter, then 50 μL (~1–5 × $10^7$ CFU) was used to infect each mouse.

### Antimicrobial susceptibility

UR34-GFP were grown for 10 h statically at 37 °C in LB. The culture was serially diluted to $10^5$ CFU/mL using GEN concentrations of 6.25-, 12.5-, 25-, 50-, 100-, and 200-μg/mL followed by incubation for 24 h at 37 °C. The minimum inhibitory concentration (MIC) was determined as the lowest concentration of antibiotic that no bacterial growth was visibly observed. From the tubes with no visible growth, 100 μL was spread onto LB agar plates and incubated overnight at 37 °C. Plates were checked for growth and the lowest concentration of antibiotic that prevented 100 % of bacterial growth was determined as the minimum bactericidal concentration (MBC).

### Ethics statement

Animal experiments were performed using protocols approved by the Institutional Animal Care and Use Committee at the University of Colorado Denver Anschutz Medical Campus (Public Health Service Animal Assurance of Compliance #D16–00171).

### Mice and I-VESIC delivery method in murine bladder

Adult male and female mice (C57BL/6 8–10 weeks old) were used in the study, and the method of delivery into the bladder was by the I-VESIC with a 24G × ¾" BD Insyte™ Autoguard™ Shield IV catheter under anesthesia and warming pad.

### Histology and evaluation of HTA-CPP treated murine bladder

Three groups of uninfected mice (N = 3) were treated with HTA-CPP (250 μg in 50 μL PBS) twice a day by I-VESIC for one day (Group 1), two days (Group 2) or untreated (Group 3; control). All groups were euthanized, and the bladders were harvested, fixed with 4 % paraformaldehyde, and further processed for myeloperoxidase (MPO) and F4–80 immunohistochemistry (IHC) staining, by the Gates Center Histology Core on the Anschutz Medical Campus. The sections were blinded, and then graded by a histopathologist using the following score scale for the relative number range of MPO and F4–80 IHC stained cells per 200× field quadrant and corresponding classfication: 0–2 cells, score = 0 (none); 3–10 cells, score = 1 (minor amounts); 11–25 cells, score = 2 (moderate amounts); 26–50 cells, score = 3 (extreme amounts).

### Nanogel tracking in murine bladders using labelled drug mimic delivery

Murine bladders were treated with HTA-CPP loaded with rhodamine B (25 μg in 50 μL PBS) as a drug mimetic delivered I-VESIC. The mice were kept under anesthesia for 15 min. Then, the bladders were emptied and washed three times via I-VESIC with 50 μL of PBS. At 15 min and 24 h post-wash, the bladders were harvested, fixed, and sectioned. Samples were dyed with Hoechst (1 μg/mL) for 15 min followed by imaging on the Zeiss Axio Observer 5 epifluorescent microscope equipped with X-Cite 200 DC for the excitation and emission wavelengths with filter set for rhodamine B ($\lambda_{ex}$ = 558 nm; $\lambda_{em}$ = 575 nm) and Hoechst ($\lambda_{ex}$ = 353 nm; $\lambda_{em}$ = 465 nm).

### Murine bladder infection

For the acute UTI model, mice were inoculated with 50 μL of $10^7$ CFU UR34-GFP by I-VESIC and were kept under anesthesia for 30 min, classified as zero days-post-infection (0 dpi). At 1 dpi and 2 dpi, urine samples were collected, serially diluted in PBS, and plated on LB agar for quantifying bacteriuria. Each day after the bladders were emptied, mice were treated twice per day for two days with 50 μL of 1 mg of GEN delivered subcutaneous (Sub-Q), 50 μL of 1 mg GEN delivered I-VESIC via HTA + GEN or HTA-CPP + GEN or left untreated. Mice that were I-VESIC-treated were kept under anesthesia for 30 min before waking and allowed to void. At 3 dpi, the bladders and kidneys were aseptically harvested and homogenized (0.025 % Triton X-100 in PBS) for bacterial titration on agar plates.

### Murine bladder infected P. aeruginosa IBCs imaging

Three additional infected mice were maintained under standard lodging conditions until 10 dpi when the bladders were aseptically harvested, rinsed and spread open on a microscope slide to be visualized. Intracellular imaging and confirmation of *P. aeruginosa* in the murine bladder was obtained using SlideBook 6.0 software on a Zeiss Axioplan II digital microscope (Intelligent Imaging Incorporated, Denver, CO, USA) with the FITC channel.

### Statistical analysis

Data analysis was performed using GraphPad Prism 8 for Windows (Version 8.4.0).

## Results

Previous work by our group has shown that a nanogel composed of 2-hydroxyethyl acrylate and urethane dimethacrylate (i.e., HAUD-nanogel) conjugated with the CGKRK CPP had the ability to cross the stratified urothelium plasma membranes.[16] CGKRK is a small peptide, which, like other CPPs that are cationic, mediates cellular internalization and has been extensively used in nanoparticle drug delivery.[23,24] However, the HAUD-nanogels were more hydrophobic and would not allow the hydrophilic antibiotic GEN to be loaded. Therefore, a different nanogel design with an increased hydrophilicity to facilitate higher GEN loading was needed. Towards this end, the water-dispersible HTA nanogel, which has been shown to load hydrophilic small-molecules with high efficiency due to the high content of hydroxyl and carboxylic acid groups for hydrogen bonding and dipole-dipole interaction, was modified via a facile one-step, solution-based, free-radical polymerization protocol using 2-hydroxyethyl acrylate, tetraethyl dimethacrylate, and acrylic acid monomers (Fig. 1).[15] The particle size of the HTA-CPP in PBS was determined to be 97.3 nm ± 0.5 nm in radius and a molecular weight of ~20 kDa. There was no significant impact on the HTA anionic zeta potential, which changed from − 7.4 mV ± 1.8 mV to − 6.4 mV ± 0.8 mV ($p$ = 0.43) after conjugating the surface with the cationic CPP.

While GEN is highly efficient in eradicating extracellular *P. aeruginosa*, it is reportedly impermeable to urothelial plasma membranes.[25,26] We hypothesized that by loading the GEN within HTA-CPP (i.e., HTA-CPP + GEN), intracellular delivery of GEN could be enhanced because of the hydrogen bonding interaction between the hydroxyl, carboxylic acid, and amine groups found between GEN and HTA nanogel. To determine the feasibility of delivering HTA + GEN and HTA-CPP + GEN into infected cells, the nanogels' encapsulation efficiency and loading capacity were assessed. The encapsulation efficiency for the HTA + GEN and HTA-CPP + GEN was 66.0 % ± 0.1 % and 60.0 % ± 8.6 % respectively. The loading capacity of GEN for HTA + GEN and HTA-CPP + GEN were similar at 13.2 % ± 0.1 % and 12.0 % ± 1.7 %, respectively. While our primary goal was to deliver HTA-CPP + GEN intracellularly, it was important to determine any interference caused by the CPP on the GEN released from the drug vehicle. Therefore, the GEN release kinetics from the HTA + GEN and HTA-CPP + GEN were assessed. In general, both the HTA + GEN and HTA-CPP + GEN exhibited a similar burst release profile at early time points and reached a maximum at 4 h (Fig. 2). Near maximum drug release from both HTA + GEN and HTA-CPP + GEN was sustained up to 8 h with a steady decline from 12 h – 96 h. These observations provided the initial kinetic parameters for delivering GEN to treat uropathogenic *P. aeruginosa* infected murine bladders in vivo.

The HTA-CPP cytotoxicity to the HTB-9 cell line after 24 h exposure was assessed. Up to 1 mg HTA-CPP had no significant effect on the cell's metabolism when compared to untreated cells ($p > 0.05$). In contrast, 10 mg HTA-CPP decreased the cellular metabolic activity significantly to ~19 % compared to the untreated cells ($p < 0.0001$; Fig. 3). These

data indicate that there is a large safe dosage range for HTA-CPP before cellular toxicity was reached in vitro.

Radioactive GEN* was used to quantify the amounts of GEN* delivered as a free drug or delivered from HTA-CPP into HTB-9 cells in 4 h. Approximately 36 % more GEN* was delivered by HTA-CPP than GEN* exogenously added to the cell culture medium ($p < 0.01$, Fig. 4). These data indicate that while free GEN* is absorbed by HTB-9 cells from the culture medium, more intracellular GEN* was delivered by the HTA-CPP.

The MIC and MBC of GEN for *P. aeruginosa* UR34-GFP for GEN were determined to estimate the GEN amount required for delivery by HTA-CPP. The MIC was 12.5 μg/mL and the MBC was 25 μg/mL. However, studies that have used GEN for systemic delivery (i.e., subcutaneous or tail-vein injection) for treating various types of infection in rodent models, including UTIs, in vivo with *P. aeruginosa* had to use a therapeutic dosage in a range of 2.5 mg/kg – 80 mg/kg, which was significantly greater than the predetermined MIC and MBC in vitro.[27–29] Therefore, in order to examine the efficacy of delivering a GEN dosage I-VESIC via HTA-CPP, we delivered 1000 μg GEN into the murine bladder (i.e., ~43 mg/kg) via Sub-Q or HTA-CPP that is within the 2.5–80 mg/kg dosage that is needed for a systemic therapeutic effect in our in vivo murine acute UTI model.

Before transitioning immediately into an in vivo murine infection model, we determined whether the antibiotic-free HTA-CPP induced an inflammatory response in healthy murine bladders. Microscopic evaluation of H&*E*-stained bladder sections that were untreated and treated with HTA-CPP for 24 h and 48 h (Fig. 5 A – C) showed evidence of minor edema in the lamina propria from each treated groups, and there was also a slight increase in urothelium thickness and sloughed cells in the murine bladder lumen. Yet, there was no sign of cell lysis. Furthermore, IHC showed there was no significant difference on the presence of murine macrophages F4–80 maker between control and HTA-CPP treated bladders at 24 h and 48 h, yet there was a slight significant difference for the presence neutrophil MPO marker between groups ($p = 0.045$), indicating that the HTA-CPP overall has a safe usage with minimal side effects (Table 1; Supplemental Figs. 1–2).

We previously demonstrated the penetration and delivery of rhodamine B into healthy murine bladders using HAUD-nanogel conjugated to the CGKRK CPP; however, HAUD-nanogel uptake required focal mechanical bladder injury.[16] Therefore, HTA-CPP loaded with rhodamine B was delivered to infected murine bladders without mechanical injury to determine whether HTA-CPP can penetrate infected murine bladder epithelium. Examination by ex vivo fluorescent imaging was performed on murine bladders untreated (control, Fig. 5 D) and post-treated by I-VESIC delivery of the rhodamine B loaded HTA-CPP at 15 min (Fig. 5 E) and 24 h (Fig. 5 F). Rhodamine B was intracellular at 15 min (Fig. 5 E) at higher relative fluorescence than background level (Fig. 5 D) and reduced to near-background levels by 24 h (Fig. 5 F), indicating that the HTA-CPP delivery system can be used to treat *P. aeruginosa*-infected murine bladders without inducing mechanical injury. These results also indicate that the rhodamine B was mostly cleared from the infected murine bladders within 24 h.

Murine bladders were infected with the uropathogenic *P. aeruginosa* clinical isolate UR34 to determine if the HTA-CPP + GEN could be used on a CAUTI pathogen. Evidence is available that *P. aeruginosa* can establish IBCs in a murine UTI model but that study was conducted with a laboratory *P. aeruginosa* strain.[5] To confirm that the clinical *P. aeruginosa* isolate UR34 was able to infect the bladders of mice, a plasmid encoding GFP was introduced into the isolate, mice were infected and urinary bladders collected to visualize the location of the bacteria. Intracellular *P. aeruginosa* UR34 were visualized by confocal microscopy residing within the murine bladder epithelium (Fig. 6).

The infected mice were treated with the same GEN dose (1 mg/mL) to compare the efficacy of HTA, HTA-CPP (I-VESIC)-delivered GEN to the subcutaneously-delivered treatment. Determination of bacteriuria is the gold standard used in the clinic for UTI diagnosis. The urines from these treatment groups were collected at 1 and 2 dpi and there was no significant difference in bacterial loads between the treatment groups at these timepoints. However, the UR34 bacterial loads from HTA-CPP + GEN-treated urines from 2 dpi trended lower in comparison to the untreated infected mice urine (Supplemental Fig. 3 A and B). Moreover, the bacteria were not detected in ~80 % of the kidneys isolated from the 3 dpi HTA-CPP + GEN treatment group (Supplemental Fig. 3C).

In order to determine if HTA-CPP + GEN was more effective at delivering GEN to the murine bladders than systemic (subcutaneous GEN) or no treatment, CFUs from these groups' bladders were quantified at 3 dpi. Comparison of the CFUs obtained from the bladders of untreated infected mice to mice treated with GEN subcutaneously showed clearance of the bacterial load from four subcutaneously antibiotic treated mice, while no mice in the untreated group cleared the infection. In contrast, there was a statistically significant difference between the untreated mice and mice treated with HTA-CPP + GEN ($p$ <0.001, Fig. 7 A). In order to determine if HTA-CPP + GEN was more effective at delivering GEN to the murine bladders than HTA without the CPP, infected mice were treated with HTA + GEN. There was significant difference between mice treated with HTA-CPP + GEN and HTA + GEN ($p$ < 0.01), and 12 of the 16 mice treated with HTA-CPP + GEN cleared the *P. aeruginosa* UR34 from their bladders as opposed to 4 of the 16 mice treated with HTA + GEN (Fig. 7 B). These results indicate that HTA-CPP + GEN was most efficacious in eliminating intracellular *P. aeruginosa*.

## Discussion

This study was initiated to develop a targeted approach for treating UTIs by enabling the localized, I-VESIC delivery of an antibiotic to the site of IBCs within the urothelium. GEN was chosen for its broad-spectrum antibiotic activity against *P. aeruginosa* and its widely reported impermeability to urothelial plasma membranes. There have been a limited number of studies examining the efficacy of nanogels conjugated with a CPP and/or nanogels carrying antibiotics for the treatment of UTIs, including CAUTI.[9–11] We synthesized a novel nanogel-CPP conjugate compatible with GEN and characterized its efficacy in treating a clinical isolate of an intracellular bacterial pathogen in a murine in vivo UTI model.

The average HTA-CPP radius was formulated at ~100 nm, within the average range of 10–200 nm for nanogels that are typically evaluated for drug delivery systems.[30] This scale ensured that the nanogels were positioned for cellular uptake. Upon determining the GEN release kinetics, the GEN loading capacity for HTA-CPP (loading capacity = ~12 %) was comparable to other GEN-loaded nanogel-based drug delivery systems that span between 6 % – 32 %.[31,32] Therefore, the loading capacities attained were deemed sufficient for this study since the final GEN amount delivered can be adjusted to attain thereapuetic doses.

An advantage of this nanogel synthesis protocol is the ease of mitigating the toxicity that arises from nano-scale particles that depends on multiple physicochemical properties.[33] While a combination of factors contribute to toxicity, toxicity increases as the radius decreases below ~50 nm.[34,35] Other factors that determine nanogel toxicity are 1) chemical composition, such as the organic and inorganic building blocks that are used to construct the nanogel, and 2) zeta potential, where studies have shown that maintaining the zeta potential between − 10 mV and + 10 mV is advantageous since it does not electrostatically attract other charged biomolecules due to a relatively ‘neutral’ charge.[13,35,36] The monomers for HTA synthesis were chosen for their low toxicity and hydrophilicity.[15,37–39] Moreover, the anionic HTA differs from other nanoparticle-based delivery approaches for treating UTIs that are relatively cationic (range + 10 mV – +20 mV).[40–43] The advantage of using cationic nanoparticles is that it can electrostatically interact with the anionic surfaces of bacteria and induce intracellular uptake, produce reactive oxygen species, disrupt bacterial membranes, deplete ATP, and impact gene and protein regulation.[44–47] However, delivering considerable amounts of these cationic nanoparticles also disrupts eukaryotic mitochondria and lysosome plasma-membranes which limits the usable concentration of nanogels.[48] Our results support the hypothesis that the HTA’s intrinsic anionic properties leads to lower cytotoxicity and better cellular uptake into the urothelial cells via the conjugated cationic CPP without significant impact, thereby permitting higher drug concentrations for treatment.

The ideal drug release kinetics for any drug delivery system is subjective and depends on multiple factors such as the disease or infection under study, target location for delivery, and the nature of the drug. For example, a burst release is a preferred mechanism to treat acute infections, while a sustained release of a drug is preferred in conditions that conventionally require frequent doses. The GEN exhibited a burst release from HTA-CPP, which is advantageous for achieiving a high dose environment, thereby killing planktonic pathogens found in the bladder lumen before it can reestablish IBCs. However, rapid drug release into the bladder prior to HTA-CPP cellular internalization is at risk for washout by urinary flow and diluting the intracellular drug availability.[49] The rapid release kinetics may explain why there was only slight statistical increase in intracellular GEN delivered by HTA-CPP in vitro versus the free GEN. A rapid release coupled with a controlled release of the drug would be more desirable for maintaining a higher intracellular GEN concentration over time, as shown by the sustained GEN release activity from the polymethysilsesquioxane capsules over days in treating another uropathogen *E. faecalis*.[9] Futhermore, controlled drug release would prevent the drug resistance evolution from having low dose exposure over time.[50] Within the current HTA, strategies for controlled GEN release, such as using specific environmental triggers (e.g., light, pH, thermal, and enzymatic) to facilitate drug release from the nanogel, are feasible and are currently being investigated by our group.[15,51]

The HTA-CPP approach towards treating UTIs is advantageous due to its targeted, local delivery and ability to penetrate the urothelium. Current standards for antibiotic therapeutics against UTIs are delivered systemically via oral or intravenous administration routes.[52] However, these practices require high doses to reach therapeutic concentrations in vivo because the bacteria reside within the urothelium. Consequently, high antibiotic doses increase harmful side effects on other organs such as the kidneys.[53] Alternatively, local drug delivery increases biodistribution at the target organ and abrogates side effects.[11] Currently, bladder instillations with GEN, which can decrease antibiotic resistance and symptomatic UTI episodes, are performed on patients with refractory UTIs when other first-line UTI therapies fail.[49] Yet, drug instillation into the bladder does not clear the infection, in part due to the bladder permeability barrier that prevents drug penetration into the underlying cells.[50] In the murine model, the HTA-CPP delivered the GEN payload I-VESIC to the bladder and cleared a majority of the *P. aeruginosa* infected murine bladders compared to other similar studies using GEN.[28,29,54] These results provide the potential for using the HTA-CPP as a drug-carrier vehicle for bladder instillations to treat UTIs in the clinic with the advantage of delivering less drug directly to the infection site and increasing drug biodistribution to the urothelium. Furthermore, the HTA-CPP are stable at room temperature and can be easily adapted for similar delivery in an office setting. However, systemic antibiotics cause side effects to patients and the emergence of antimicrobial resistance in uropathogenic bacteria.

GEN is a broad-spectrum antibiotic that is typically used for moderate to severe infections, particularly against Gram-negative organisms and is considered to be a non-membrane permeable antibiotic.[25,26] However, several studies have used different methods to make GEN permeable to bladder epithelia. For instance, Gomarasca et al.[55] used a CPP-conjugated GEN treatment to kill intracellular *E. coli* K1 RS218 and reported a significant reduction of the intracellular bacteria. Kim et al.[56] demonstrated GEN can enter into host cells in vitro, presumably through pinocytosis, leading to inaccurate numbers of intracellular CFU, thereby indicating significant variations on the outcome. Additionally, Blango and Mulvey[57] used GEN as one of many antibiotics to treat against the clinical isolate bacterial strain, UTI89-GFP. The study demonstrated that GEN reduced, but did not eliminate, the uropathogenic *Escherichia coli* CFUs in biofilm and within host urothelial cells; the combination of biofilm formation physiology and the urothelial cell barrier were cited as likely causes for uropathogenic *Escherichia coli* resistance to GEN treatment. These causes may be applicable here for the pathogensis of UR34 where the IBCs established as biofilms in the urothelial cell's cytoplasm and could have a subset of pathogens establishing long-term reservoirs in endosomal-lysosomal vesicles.[58] Additional cell-compartment targeting molecules like lysosomol sorting peptides have shown promise for improving target drug delivery to accomplish uropathogen eradication while reducing antimicrobial resistance and side effects from drugs delivered systemically.[59] In the future, more CPP conjugated on the nanogel, different CPPs, or nanogels containing biofilm-disrupting molecules or antimicrobial peptides could be explored as alternatives for improvement.

Overall, our findings demonstrate that the novel, cell-compatible HTA nanogel conjugated with the CGKRK CPP can be loaded with GEN to successfully penetrate the urothelium and

target uropathogenic *P. aeruginosa* for eradication from the murine bladder, highlighting it as a potential nanogel-based drug delivery approach to treat UTIs.

## Supplementary Material

Refer to Web version on PubMed Central for supplementary material.

## Acknowledgments

The authors acknowledge Dr. Allen Hauser at Northwestern University, Feinberg School of Medicine for the *P. aeruginosa* clinical isolate UR34. We also thank Hannah Dimmick from the Department of Obstetrics and Gynecology at University of Colorado School of Medicine for her service in proofreading the manuscript. Furthermore, we thank the Gates Center Histology Core on the Anschutz Medical Campus for processing H&E samples. This work was funded by the SPARK Collaboratory Program at CU Anschutz Medical Campus, the National Institute of Allergy and Infectious Diseases Grant (1R21AI154360-01, T32AI052066), NIH-NIDCR (1R21DE032135-01A1) and the Veterans Administration (BX0002073, IK6BX005384). This work is based on US Patent 11,642,319-B2 (2023) “Targeted Nanogels for Urinary Bladder Therapies” by inventors: Devatha P. Nair, Dmitri Simberg, and Manju Saraswathy.

## Data availability

The data that support the findings of this study are available from the corresponding author upon reasonable request.

## References

1. Foxman B Urinary tract infection syndromes: occurrence, recurrence, bacteriology, risk factors, and disease burden. Infectious Disease Clinics. 2014;28(1):1–13. [PubMed: 24484571]
2. Ronald A The etiology of urinary tract infection: traditional and emerging pathogens. Disease-a-Month. 2003;49(2):71–82. [PubMed: 12601338]
3. Foxman B Epidemiology of urinary tract infections: incidence, morbidity, and economic costs. Am J Med. 2002;113(1, Supplement 1):5–13.
4. Foxman B The epidemiology of urinary tract infection. Nat Rev Urol. 2010;7(12): 653–660. [PubMed: 21139641]
5. Penaranda C, Chumbler NM, Hung DT. Dual transcriptional analysis reveals adaptation of host and pathogen to intracellular survival of Pseudomonas aeruginosa associated with urinary tract infection. PLoS Pathog. 2021;17(4). p. e1009534. [PubMed: 33901267]
6. Newman JW, Floyd RV, Fothergill JL. The contribution of Pseudomonas aeruginosa virulence factors and host factors in the establishment of urinary tract infections. FEMS Microbiol Lett. 2017;364(15). p. fnx124.
7. Medina M, Castillo-Pino E. An introduction to the epidemiology and burden of urinary tract infections. Ther Adv Urol. 2019;11. p. 1756287219832172. [PubMed: 31105774]
8. Hassett DJ, et al. The bactericidal tandem drug, AB569: how to eradicate antibiotic-resistant biofilm pseudomonas aeruginosa in multiple disease settings including cystic fibrosis, burns/wounds and urinary tract infections. Front Microbiol. 2021;12.
9. Labbaf S, et al. An encapsulated drug delivery system for recalcitrant urinary tract infection. Journal of The Royal Society Interface. 2013;10(89):20130747. [PubMed: 24068180]
10. Gao W, et al. Nanoparticle-based local antimicrobial drug delivery. Adv Drug Deliv Rev. 2018;127:46–57. [PubMed: 28939377]
11. Mittal R, et al. Local drug delivery in the urinary tract: current challenges and opportunities. J Drug Target. 2018;26(8):658–669. [PubMed: 29251520]
12. Soni KS, Desale SS, Bronich TK. Nanogels: an overview of properties, biomedical applications and obstacles to clinical translation. J Control Release. 2016;240: 109–126. [PubMed: 26571000]

13. Verma A, Stellacci F. Effect of surface properties on nanoparticle–cell interactions. Small. 2010;6(1):12–21. [PubMed: 19844908]
14. Zhang L, et al. Interplay of nanoparticle rigidity and its translocation ability through cell membrane. J Phys Chem B. 2019;123(42):8923–8930. [PubMed: 31566375]
15. Escobedo HD, Stansbury JW, Nair DP. Photoreactive nanogels as versatile polymer networks with tunable in situ drug release kinetics. J Mech Behav Biomed Mater. 2020;108, 103755. [PubMed: 32310108]
16. Griffin JI, et al. Cell-penetrating peptide CGKRK mediates efficient and widespread targeting of bladder mucosa following focal injury. Nanomedicine: Nanotechnology, Biology and Medicine. 2017;13(6):1925–1932. [PubMed: 28428051]
17. Catania R, et al. Study on significance of receptor targeting in killing of intracellular bacteria with membrane-impermeable antibiotics. Advanced Therapeutics. 2021;4 (12):2100168.
18. Gubernator J, Drulis-Kawa Z, Kozubek A. A simply and sensitive fluorometric method for determination of gentamicin in liposomal suspensions. Int J Pharm. 2006;327(1):104–109. [PubMed: 16935441]
19. Ritsema JAS, et al. Relationship between polarities of antibiotic and polymer matrix on nanoparticle formulations based on aliphatic polyesters. Int J Pharm. 2018;548 (2):730–739. [PubMed: 29133206]
20. D'Souza S A review of in vitro drug release test methods for nano-sized dosage forms. Advances in Pharmaceutics. 2014;2014(1):304757.
21. Postma A, et al. Self-polymerization of dopamine as a versatile and robust technique to prepare polymer capsules. Chem Mater. 2009;21(14):3042–3044.
22. Diver JM, Bryan LE, Sokol PA. Transformation of Pseudomonas aeruginosa by electroporation. Anal Biochem. 1990;189(1):75–79. [PubMed: 2126169]
23. Ruoslahti E Peptides as targeting elements and tissue penetration devices for nanoparticles. Adv Mater. 2012;24(28):3747–3756. [PubMed: 22550056]
24. Hu Q, et al. CGKRK-modified nanoparticles for dual-targeting drug delivery to tumor cells and angiogenic blood vessels. Biomaterials. 2013;34(37):9496–9508. [PubMed: 24054848]
25. Rosenkrantz BE, Greco JR, Hoogerheide JG, Oden EM. Gentamicin Sulfate. In: Florey K, ed. Analytical Profiles of Drug Substances. Academic Press; 1981:295–340.
26. Tangy F, et al. Mechanism of action of gentamicin components. Eur J Biochem. 1985; 147(2):381–386. [PubMed: 3882427]
27. Goering Richard V, Sanders Christine C, Sanders WE. Comparison of 5-Episisomicin (Sch 22591), gentamicin, Sisomicin, and tobramycin in treatment of experimental Pseudomonas infections in mice. Antimicrob Agents Chemother. 1978;14(6):824–828. [PubMed: 742870]
28. Nicas TI, Bryan LE. Relationship between gentamicin susceptibility criteria and therapeutic serum levels for Pseudomonas aeruginosa in mouse infection model. Antimicrob Agents Chemother. 1978;13(5):796–801. [PubMed: 96735]
29. LeBrun M, et al. Effectiveness and toxicity of gentamicin in an experimental model of pyelonephritis: effect of the time of administration. Antimicrob Agents Chemother. 1999;43(5):1020–1026. [PubMed: 10223909]
30. HKS Y, NA AH, and GA A. Nanogels as Novel Drug Delivery Systems - A Review. Journal of Pharmacy and Pharmaceutical Research. 2017;1(1:5).
31. Zabihian A, et al. Preparation of composite nanogel carrier for gentamicin delivery. Research in Pharmaceutical Sciences. 2012;7(5).
32. Zabihian A, Salouti M, Hamidi M. Factorial design analysis and optimisation of chitosan-based nanogels as controlled release system for gentamicin. IET Nanobiotechnol. 2018;12(1):12–17.
33. Sayes CM, Warheit DB. Characterization of nanomaterials for toxicity assessment. WIREs Nanomedicine and Nanobiotechnology. 2009;1(6):660–670. [PubMed: 20049823]
34. Oyewumi MO, Kumar A, Cui Z. Nano-microparticles as immune adjuvants: correlating particle sizes and the resultant immune responses. Expert Rev Vaccines. 2010;9(9):1095–1107. [PubMed: 20822351]

35. Shang L, Nienhaus K, Nienhaus GU. Engineered nanoparticles interacting with cells: size matters. J Nanobiotechnol. 2014;12(1):5.
36. Srivastava V, Gusain D, Sharma YC. Critical review on the toxicity of some widely used engineered nanoparticles. Industrial & Engineering Chemistry Research. 2015;54 (24):6209–6233.
37. Wilems TS, et al. Effects of free radical initiators on polyethylene glycol dimethacrylate hydrogel properties and biocompatibility. J Biomed Mater Res A. 2017;105(11):3059–3068. [PubMed: 28744952]
38. Siafaka PI, et al. Porous dressings of modified chitosan with poly(2-hydroxyethyl acrylate) for topical wound delivery of levofloxacin. Carbohydr Polym. 2016;143: 90–99. [PubMed: 27083347]
39. Xu M, et al. Improved in vitro and in vivo biocompatibility of graphene oxide through surface modification: poly(acrylic acid)-functionalization is superior to PEGylation. ACS Nano. 2016;10(3):3267–3281. [PubMed: 26855010]
40. Slavin YN, Asnis J, Häfeli UO, Bach H. Metal nanoparticles: understanding the mechanisms behind antibacterial activity. J Nanobiotechnol. 2017;15(1):65.
41. Divya M, Kiran GS, Hassan S, Selvin J. Biogenic synthesis and effect of silver nanoparticles (AgNPs) to combat catheter-related urinary tract infections. Biocatal Agric Biotechnol. 2019;18:101037.
42. Lopez-Carrizales M, et al. In vitro synergism of silver nanoparticles with antibiotics as an alternative treatment in multiresistant uropathogens. Antibiotics. 2018;7. 10.3390/antibiotics7020050.
43. Rodríguez-Serrano C, et al. Biosynthesis of silver nanoparticles by fusarium scirpi and its potential as antimicrobial agent against uropathogenic Escherichia coli biofilms. PloS One. 2020;15(3). p. e0230275. [PubMed: 32163495]
44. Naqvi SZ, et al. Combined efficacy of biologically synthesized silver nanoparticles and different antibiotics against multidrug-resistant bacteria. Int J Nanomedicine. 2013;8:3187–3195. [PubMed: 23986635]
45. Payne JN, et al. Novel synthesis of kanamycin conjugated gold nanoparticles with potent antibacterial activity. Front Microbiol. 2016;7.
46. Morones-Ramirez JR, Winkler JA, Spina CS, Collins JJ. Silver enhances antibiotic activity against gram-negative bacteria. Sci Transl Med. 2013;5(190). p. 190ra81–190ra81.
47. Woźniak-Budych MJ, et al. Green synthesis of rifampicin-loaded copper nanoparticles with enhanced antimicrobial activity. J Mater Sci Mater Med. 2017;28 (3):42. [PubMed: 28150115]
48. Fröhlich E The role of surface charge in cellular uptake and cytotoxicity of medical nanoparticles. Int J Nanomedicine. 2012;7:5577–5591. [PubMed: 23144561]
49. Pichl CM, et al. Biomimickry of UPEC cytoinvasion: a novel concept for improved drug delivery in UTI. Pathogens. 2016;5. 10.3390/pathogens5010016.
50. Tyagi P, et al. Recent advances in intravesical drug/gene delivery. Mol Pharm. 2006; 3(4):369–379. [PubMed: 16889430]
51. Ahmed S, Alhareth K, Mignet N. Advancement in nanogel formulations provides controlled drug release. Int J Pharm. 2020;584:119435. [PubMed: 32439585]
52. Ventola CL. The antibiotic resistance crisis: part 2: management strategies and new agents. P t. 2015;40(5):344–352. [PubMed: 25987823]
53. Arora D, et al. An update on polysaccharide-based nanomaterials for antimicrobial applications. Appl Microbiol Biotechnol. 2016;100(6):2603–2615. [PubMed: 26830099]
54. Hopkins Walter J, Gendron-Fitzpatrick A, Balish E, Uehling David T. Time course and host responses to Escherichia coli urinary tract infection in genetically distinct mouse strains. Infect Immun. 1998;66(6):2798–2802. [PubMed: 9596750]
55. Gomarasca M, et al. Bacterium-derived cell-penetrating peptides deliver gentamicin to kill intracellular pathogens. Antimicrob Agents Chemother. 2017;61(4). 10.1128/aac.02545-16.
56. Kim J-H, et al. Alternative enzyme protection assay to overcome the drawbacks of the gentamicin protection assay for measuring entry and intracellular survival of staphylococci. Infect Immun. 2019;87(5). 10.1128/iai.00119-19.

57. Blango Matthew G, Mulvey Matthew A. Persistence of Uropathogenic Escherichia coli in the face of multiple antibiotics. Antimicrob Agents Chemother. 2010;54(5): 1855–1863. [PubMed: 20231390]

58. Wang C, et al. Atg16L1 deficiency confers protection from uropathogenic Escherichia coli infection in vivo. Proc Natl Acad Sci U S A. 2012;109(27): 11008–11013. [PubMed: 22715292]

59. Dekiwadia CD, Lawrie AC, Fecondo JV. Peptide-mediated cell penetration and targeted delivery of gold nanoparticles into lysosomes. J Pept Sci. 2012;18(8): 527–534. [PubMed: 22764089]

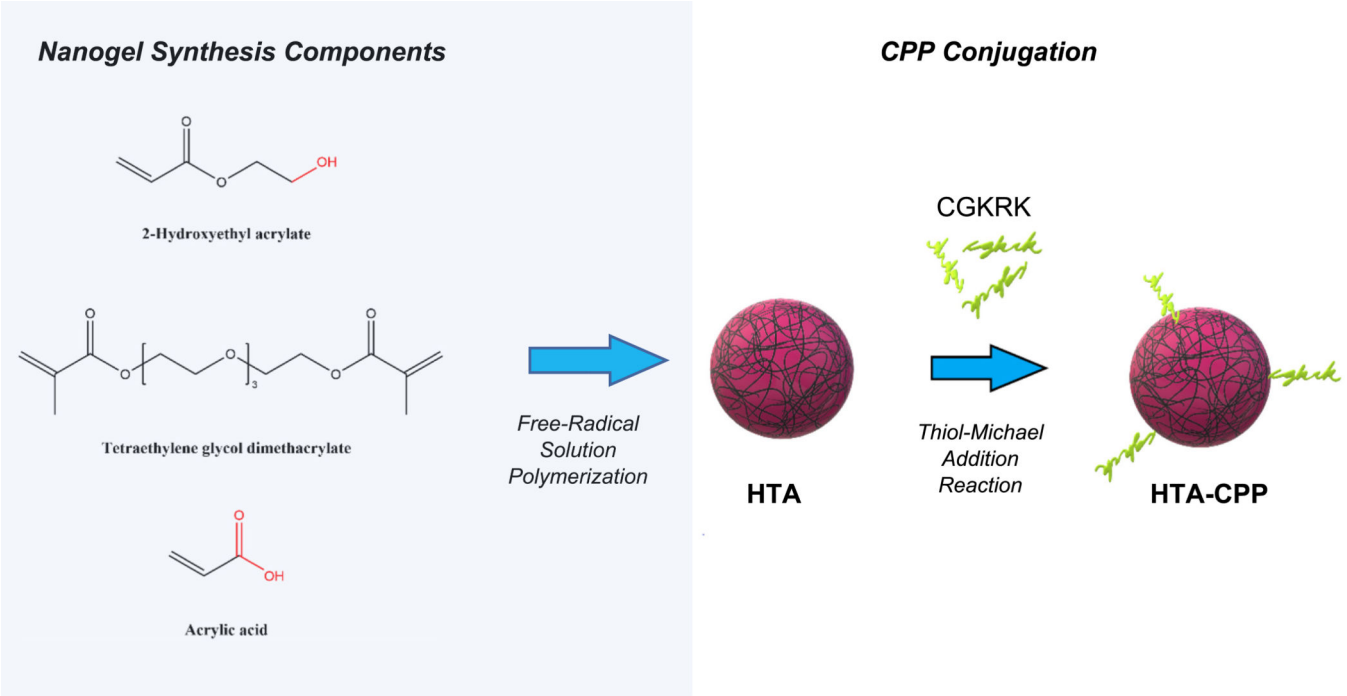


**Fig. 1. Overview for the composition and synthesis of HTA-CPP.**

Composition of HTA nanogel synthesized after free-radical solution polymerization followed by conjugating the cell-penetrating peptide (CPP) Cys-Gly-Lys-Arg-Lys (CGKRK) onto the nanogel's surface nanogel (HTA-CPP) for loading and delivering the gentamicin antibiotic in the HTA-CPP.

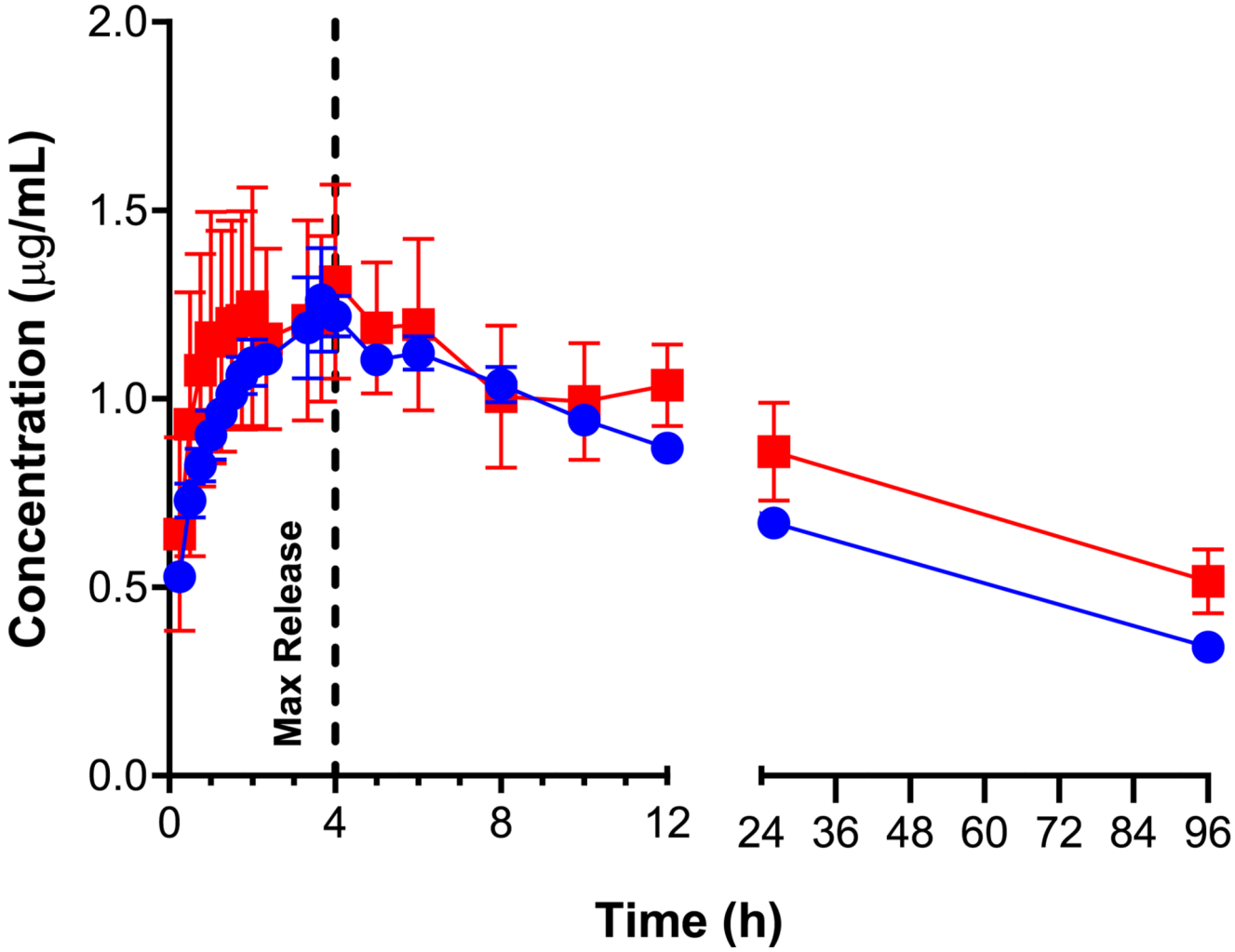


**Fig. 2. Gentamicin release kinetics from the HTA and HTA-CPP.**

Gentamicin released from the HTA-CPP (red, squares) and HTA (blue, circles) at 37 °C in PBS via dialysis method. Gentamicin release was measured by spectroscopy of fluorescently derivatized GEN as described in the Materials and Methods every 2 h to 12 h, 24 h and 96 h. Error bars are the standard deviation for N = 3.

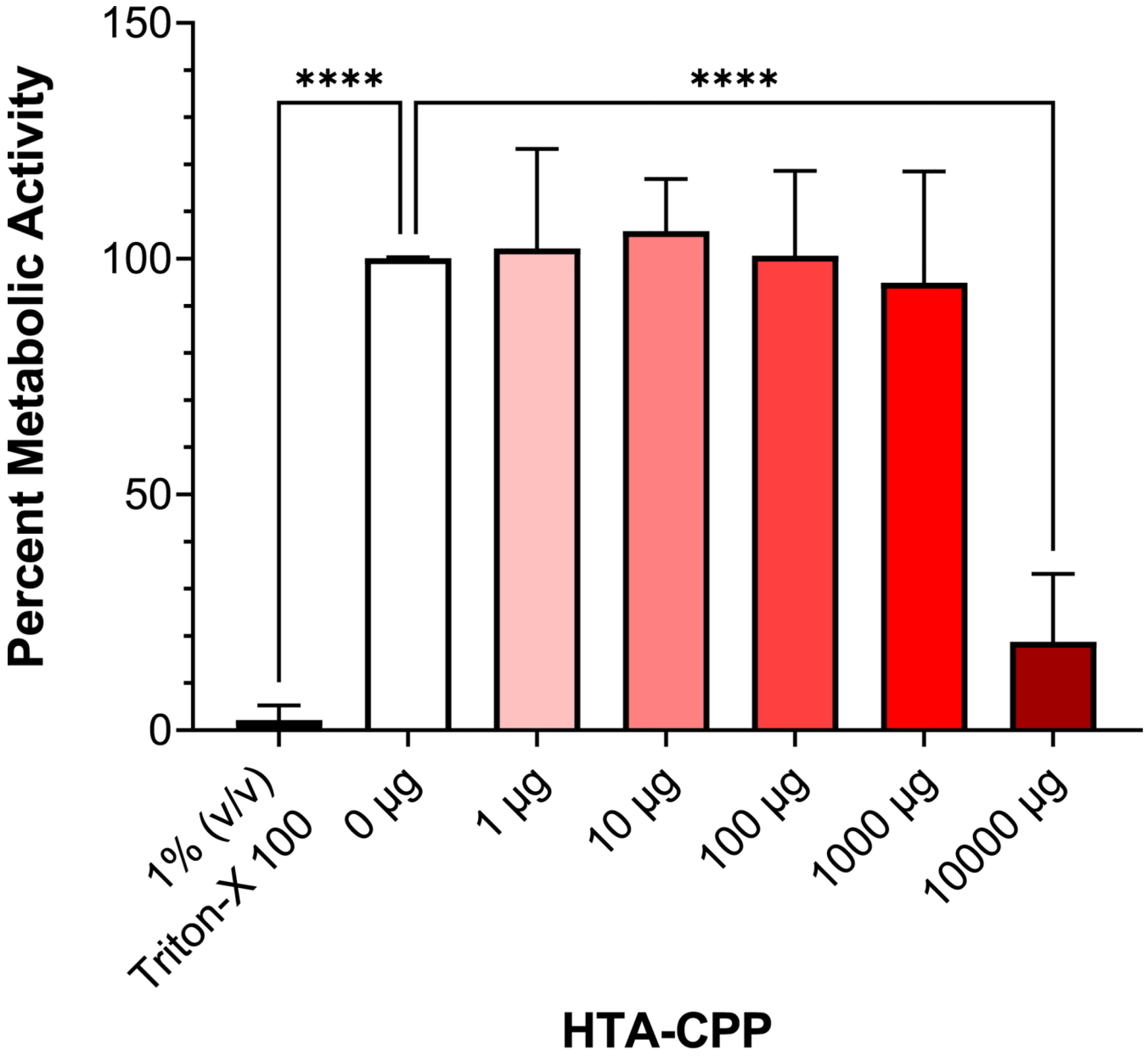


**Fig. 3. Effects of HTA-CPP concentrations on urothelial cell viability.**

The metabolic activity of human urothelial cells (HTB-9) was determined by MTT assay after 24 h exposure to the HTA conjugated to the CPP (HTA-CPP). Cells were exposed to 1 % (v/v) Triton X-100 as a positive control. Cells that were not exposed to HTA-CPP (0 µg) was the negative control. Percent metabolic activity was determined as described in Materials and Methods. Error bars are the standard devitation for N = 3. One-way ANOVA woth post-hoc Dunnett's multiple comparison test; ****, $p < 0.0001$.

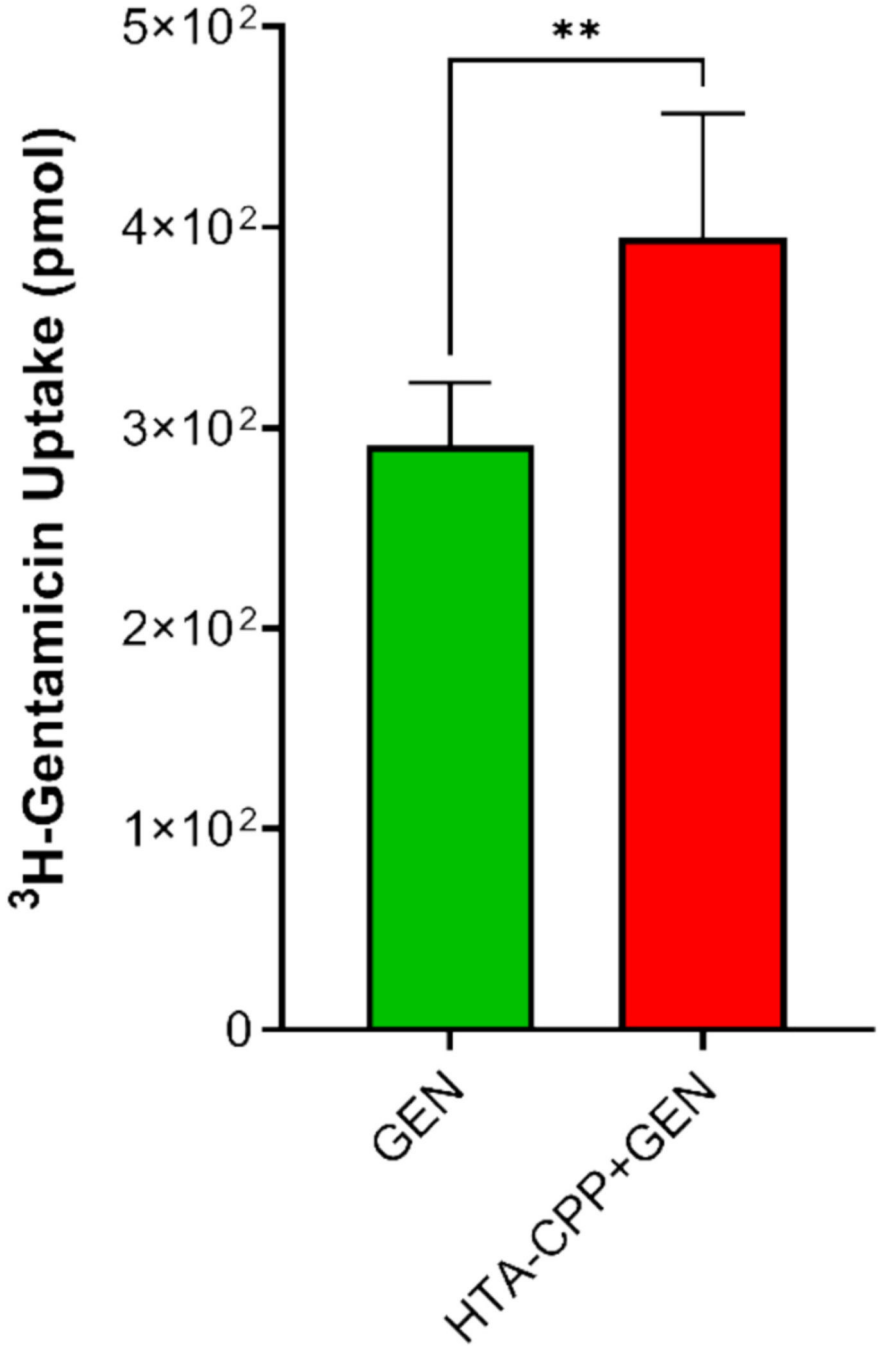


**Fig. 4. Gentamicin absorption by human urothelial cells delivered as free drug vs. encapsulated in HTA-CPP.**

The amount of intracellular radioactive $^{3}$H-gentamicin in human urothelial cells (HTB-9) by counts-per-minute from lysed cells after $^{3}$H-gentamicin was delivered either as a free drug in solution (GEN, green bar) or by HTA-CPP (HTA-CPP + GEN, red bar) after 4 h. Student t-test; **, $p < 0.01$.

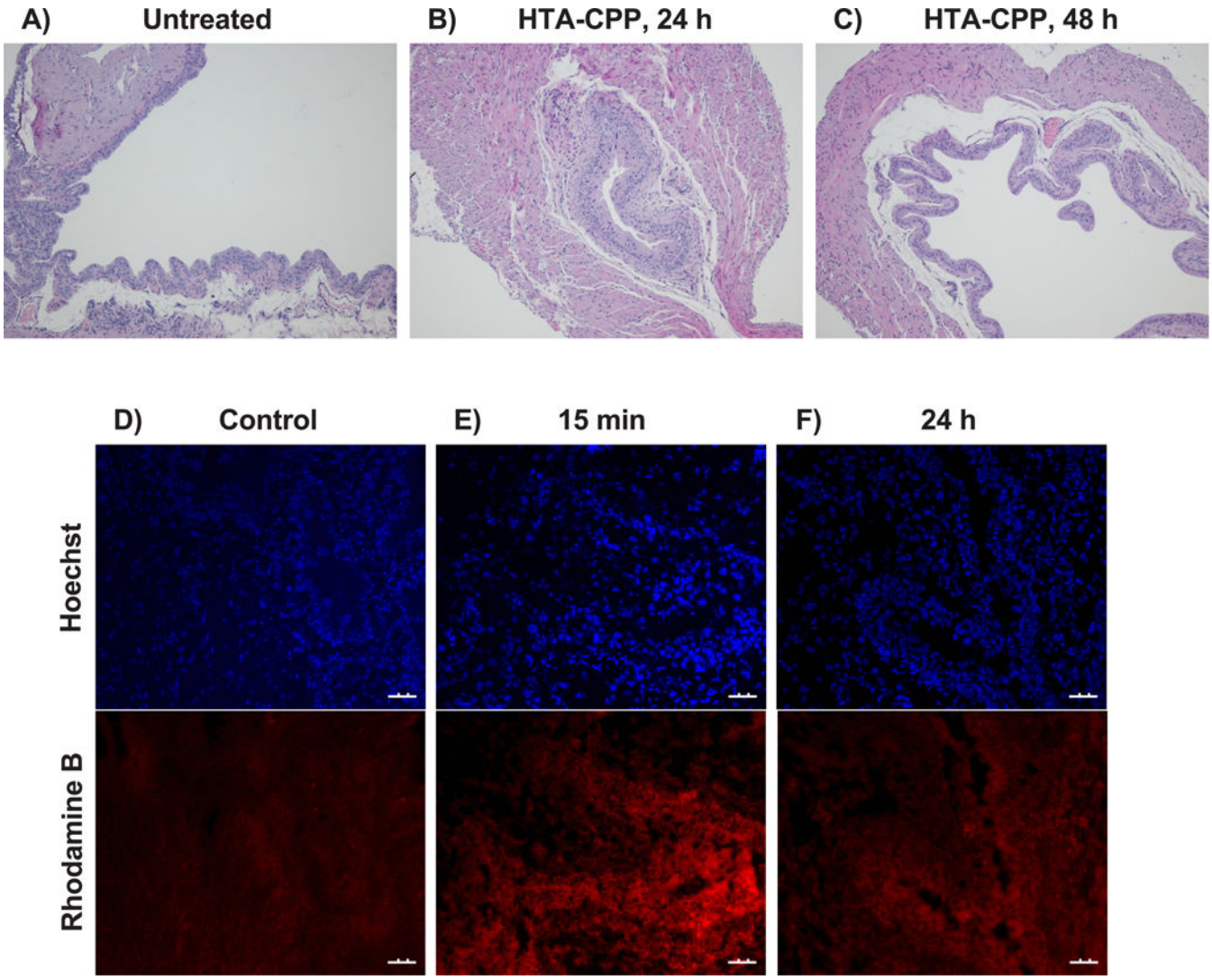


**Fig. 5. Effects of HTA-CPP on murine bladders.**

Representative images of hematoxylin and eosin-stained murine bladders that were (A) untreated and treated with HTA-CPP (250 μg), after (B) 24 h, and (C) 48 h (magnification 100×). Representative images of harvested infected murine bladders of (D) untreated (control) and post (E) 15 min and (F) 24 h intravesical treatment with rhodamine B payload from HTA-CPP. Rhodamine channel for rhodamine B molecule (red; nm; nm) and Hoechst channel for nuclei (blue; nm; nm).

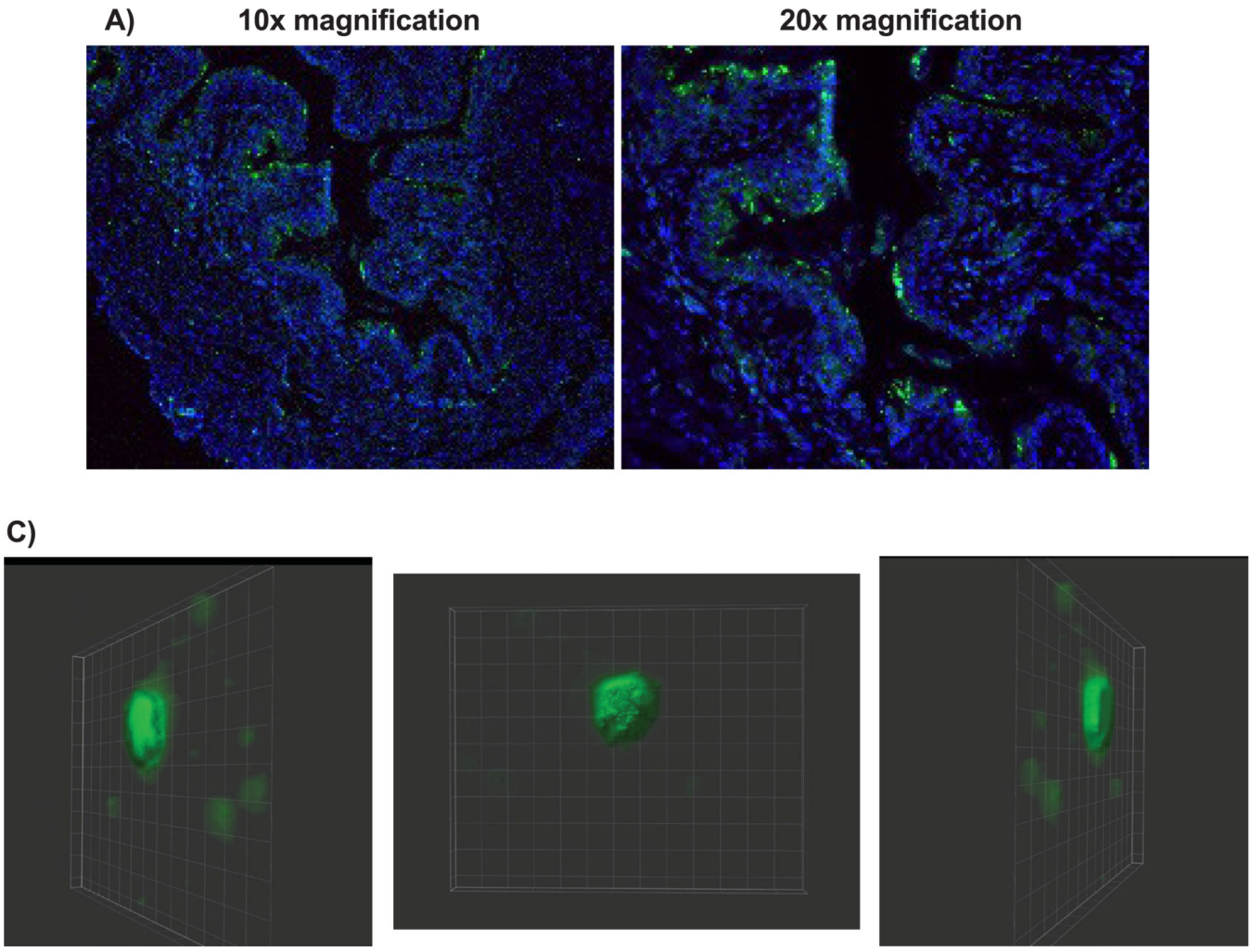


**Fig. 6. Intracellular *P. aeruginosa* within murine bladder.**

Representative images of (A) *P. aeruginosa* UR34-GFP infected murine bladders at 10 dpi and (C) *Z*-stack images of *P. aeruginosa* intracellular bacterial community. FITC channel for UR34-GFP and DAPI channel for nuclei of murine bladder.

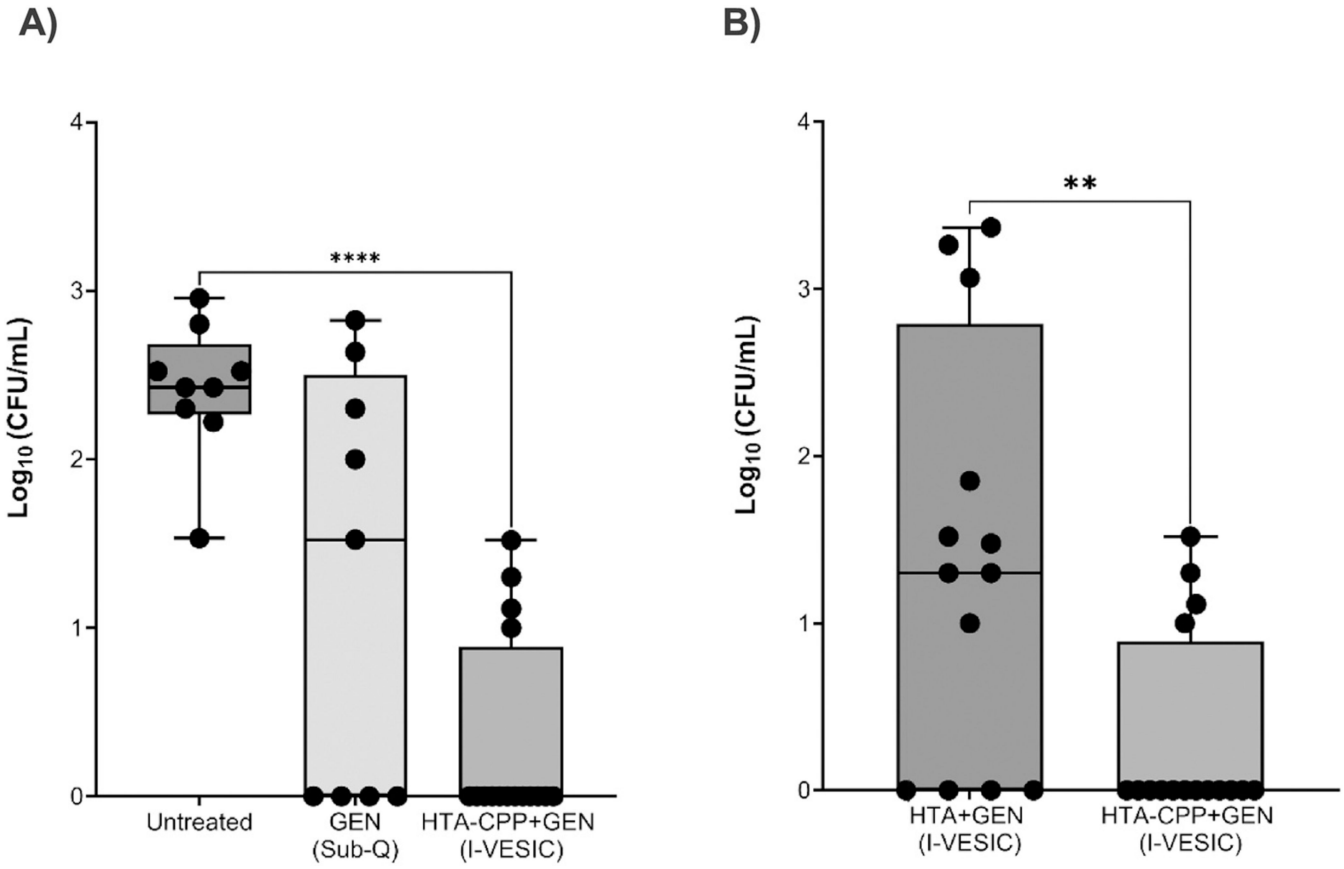


**Fig. 7. Effect of subcutaneous gentamicin, HTA + GEN and HTA-CPP + GEN on murine *P. aeruginosa* infected bladders.**

Bacterial quantification from uropathogenic *P. aeruginosa* (UR34-GFP)-infected murine bladders at 3 dpi for (A) untreated (N = 9) and treated subcutaneous (Sub-Q) delivery 1000 μg GEN (N = 9), treated HTA-CPP + GEN (N = 16) by I-VESIC (1000 μg GEN delivered), and for (B) treated HTA + GEN (N = 13) intravesically (I-VESIC) (1000 μg GEN delivered) in comparison to HTA-CPP + GEN group. Box and whisker plot with horizontal line for the median between the interquartile range and minimum/maximum extremes. Kruskal-Wallis one-way ANOVA with post-hoc Dunn's multiple comparison test against untreated and Mann Whitney test respectively; **, $p < 0.01$; **** $p < 0.0001$.

**Table 1**

Histopathological and Inflammatory marker scoring of murine bladders.

| | Average Score | | |
|---|---|---|---|
| | **Control** | **HTA-CPP, 24 h** | **HTA-CPP, 48 h** |
| Physical Characteristics | | | |
| Lumen | | | |
| *Sloughed Cells* | 0.0 | 1.0 | 0.3 |
| *Urothelium* | | | |
| *Thickness (# of cell layers)* | 2–3 | 3–4 | 3–4 |
| *Damage* | 0.0 | 0.0 | 0.0 |
| Lamina Propria | | | |
| *Edema* | 0.0 | 0.6 | 1.2 |
| Inflammation Markers | | | |
| *F4−80* | 1.4 ± 0.60 | 1.9 ± 0.93 * | 1.8 ± 1.16 |
| *MPO* | 0.0 ± 0.07 | 0.6 ± 0.52 | 0.5 ± 0.60 |

Murine bladders were scored for physical characteristics (number of cells into the lumen of the bladder, thickness of the urothelium and amount of edema in the lamina propria) and inflammation (number of macrophages using F4–80 and neutrophils using MPO) in untreated mice and HTA-CPP treated mice bladders for 24 and 48 hrs. Values for physical characteristics expressed as averages. Inflammation markers score values expressed as averages with standard deviation based on number of stained cells per 200x field quadrant. Scoring scale is based on the following values and corresponding classification: 0–2 cells, score = 0 (none); 3–10 cells, score = 1 (minor amounts); 11–25 cells, score = 2 (moderate amounts); 26–50 cells, score = 3 (extreme amounts). One-way Brown-Forsythe ANOVA test

* $p = 0.045$.